View metadata, citation and similar papers at core.ac.uk

brought to you by CORE

provided by Warwick Research Archives Portal Repository

Quantitative Local Probing of Polarization with Application on HfO_2-Based Thin Films

Owoong Kwon, Seunghun Kang, Sanghyun Jo, Yun Do Kim, Hee Han, Yeehyun Park, Xiaoli Lu, Woo Lee, Jinseong Heo, Marin Alexe, and Yunseok Kim**

Owing to their switchable spontaneous polarization, ferroelectric materials have been applied in various fields, such as information technologies, actuators, and sensors. In the last decade, as the characteristic sizes of both devices and materials have decreased significantly below the nanoscale, the development of appropriate characterization tools became essential. Recently, a technique based on conductive atomic force microscopy (AFM), called AFM-positive-up-negative-down (PUND), is employed for the direct measurement of ferroelectric polarization under the AFM tip. However, the main limitation of AFM-PUND is the low frequency (i.e., on the order of a few hertz) that is used to initiate ferroelectric hysteresis. A significantly higher frequency is required to increase the signal-to-noise ratio and the measurement efficiency. In this study, a novel method based on high-frequency AFM-PUND using continuous waveform and simultaneous signal acquisition of the switching current is presented, in which polarization–voltage hysteresis loops are obtained on a high-polarization $BiFeO_3$ nanocapacitor at frequencies up to 100 kHz. The proposed method is comprehensively evaluated by measuring nanoscale polarization values of the emerging ferroelectric $Hf_{0.5}Zr_{0.5}O_2$ under the AFM tip.

1. Introduction

Ferroelectric materials are applied in various fields, such as information technologies,[1,2] actuators,[3,4] and sensors,[5,6] owing to their unique physical properties including switchable spontaneous polarization.[7] Recently, the characteristic size of these materials has been decreased because of the increased demand for miniaturized devices, leading to reduced thickness of even HfO_2-based films of only one nanometer.[8–11] Therefore, evaluation of ferroelectricity involves considerable challenges, more than before, because the ferroelectric properties, such as the polarization value (charge density) and its switchability, must be studied at the nanoscale level.

The mapping of ferroelectric polarization at the nanoscale has been performed using piezoresponse force microscopy (PFM), which is a variation of atomic force microscopy (AFM). By detecting surface displacement induced by converse piezoelectric effect according to the application of ac voltage,[12–15] the orientation of polarization and magnitude of the local piezoelectric response can be obtained from PFM measurements. However, it has recently been revealed that non-ferroelectric contributions, such as electrostatic effect, electrostriction, and ionic motion,[16–18] can also contribute to the PFM signal. Several attempts have been made to differentiate the ferroelectric effect from the non-ferroelectric ones.[15,18,19]

O. Kwon, S. Kang, Y. Park, Y. Kim
School of Advanced Materials and Engineering
Sungkyunkwan University (SKKU)
Suwon 16419, Republic of Korea
E-mail: yunseokkim@skku.edu

S. Jo, J. Heo
Samsung Advanced Institute of Technology
Suwon 16678, Republic of Korea

Y. D. Kim
Department of Nano Science
University of Science and Technology (UST)
Daejeon 34113, Republic of Korea

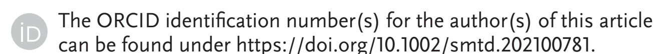
The ORCID identification number(s) for the author(s) of this article can be found under https://doi.org/10.1002/smtd.202100781.

© 2021 The Authors. Small Methods published by Wiley-VCH GmbH. This is an open access article under the terms of the Creative Commons Attribution License, which permits use, distribution and reproduction in any medium, provided the original work is properly cited.

DOI: 10.1002/smtd.202100781

H. Han
National Nano Fab Center (NNFC)
Daejeon 34141, Republic of Korea

X. Lu
School of Microelectronics & State Key Discipline Laboratory of Wide Bandgap Semiconductor Technology
Xidian University
Xi'an 710071, China

W. Lee
Korea Research Institute of Standards and Science (KRISS)
Daejeon 34113, Republic of Korea

M. Alexe
Department of Physics
The University of Warwick
Coventry CV4 7AL, UK
E-mail: M.Alexe@warwick.ac.uk

To overcome these drawbacks, conductive AFM-based techniques using the positive-up-negative-down method (AFM-PUND) have been developed for direct measurements of ferroelectric polarization.[20,21] These approaches enable investigation of ferroelectricity, and a quantitative polarization value can be obtained even through AFM. However, these methods were developed only in the low frequency range, i.e., typically on the order of a few hertz up to 1 kHz. Although ferroelectricity could be probed at the nanoscale level in these studies, evaluation of a small polarization value (i.e., weak ferroelectricity) remains challenging owing to the low signal-to-noise ratio. Thus, development of a high-frequency version of AFM-PUND would bring a series of advantages, such as reducing the noise floor by decreasing the leakage current or electrical $1/f$ noise by increasing the measuring frequency.[22] In turn, it can be used to accurately evaluate weak ferroelectricity. Furthermore, as the write/read speed directly depends on the device performance of ferroelectric-based memories, high-frequency measurement could be more relevant to device applications.[23]

In this study, we developed AFM-PUND with a continuous-type waveform in the 100-kHz range without any other circuits and applied it to an emerging material, namely a $Hf_{0.5}Zr_{0.5}O_2$ (HZO) thin film, which is relevant for next-generation nonvolatile memories. This approach can be used for powerful and simple investigation of the presence of weak ferroelectricity at the nanoscale level.

2. Results and Discussion

The sequence of conventional PUND with a continuous waveform comprises *P*, *U*, *N*, and *D*, as shown in **Figure 1**a. Prior to the application of a *P* (*N*) waveform, negative (positive) pre-poling bias was applied to align the domain in a specific direction. Then, when the *P* (*N*) waveform was applied, both switching and non-switching currents were obtained. Notably, the non-switching current includes dielectric current and leakage current.[21] Subsequently, the non-switching current was generated with the subsequent application of a *U* (*D*) waveform as switching already occurred under application of the first *P* (*N*) waveform. As a result, the current generated only by the polarization switching could be distinguished by subtracting the *U* (*D*) current from the *P* (*N*) current. The entire polarization–voltage (*P*–*V*) hysteresis loop can be reconstructed through normalization to the switched area or electrode size.

We also applied the conventional PUND to the AFM-PUND measurement. However, unlike the continuous waveform in the conventional PUND, the pulse-type waveform (Figure 1c) was used to perform the AFM-PUND measurement, as in the previous report.[21] We observed that the shape of the waveform can affect the obtained current. Thus, we comparatively evaluated the current obtained through applications of continuous- and pulse-type waveforms to determine the more suitable waveform for the high-frequency measurement. As the current was proportional to the rate of increasing variation of the applied voltage, the non-switching current was linearly proportional to the applied voltage for the pulse-type waveform (Figure 1e), which remained constant as the sign for the continuous-type waveform changed (Figure 1f). In fact, we obtained such *I*–*V* curves in the capacitor of 15 µF, which was our model system,

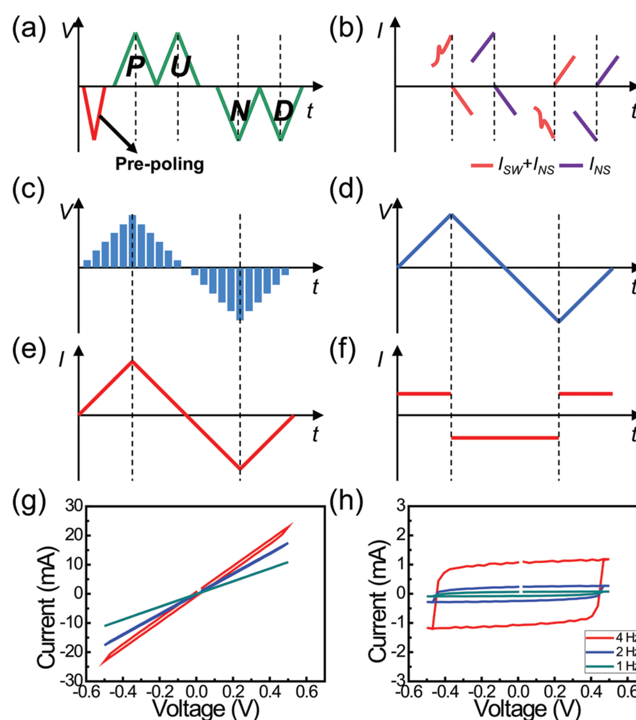

Figure 1. Schematics of PUND method with a) continuous waveform and b) corresponding *I-t* curve. Schematics of c) pulse- and d) continuous-type triangular waveforms and corresponding current behavior in capacitor by applying e) pulse- and f) continuous-type waveforms. g,h) *I*–*V* curves for capacitance of 15 µF with pulse- and continuous-type triangular waveforms.

as shown in Figures 1g,h. For both cases, the maximum non-switching current increased with increasing frequency. However, at the same frequency, the maximum non-switching current of the pulse-type waveform was much higher than that of the continuous waveform. For example, at 4 Hz, the maximum non-switching current of the pulse-type waveform was ≈20 times higher than that of the continuous waveform. If the switching current was assumed to be the same for both cases, the lower maximum non-switching current can be beneficial while considering the current amplification. This is because operation of the current amplifier with higher transimpedance gain value results in a higher signal-to-noise level than that with a lower transimpedance gain. By reducing the level of non-switching current, the resolution of the obtained switching current can be increased. Therefore, the continuous-type waveform can be favorable for high-frequency measurement of AFM-PUND.

To explore the continuous-type waveform of the AFM-PUND, we first performed PFM hysteresis loop measurements in $BiFeO_3$ (BFO) nanocapacitors, wherein the thickness of the BFO thin film was 90 nm, while the radius and thickness of the Pt electrode were 190 and 25 nm, respectively. As presented in **Figure 2**a, switchable behavior was clearly observed with a strong piezoresponse, and the coercive voltage was around 1.5 V. Then, we applied the continuous-type waveform to the BFO nanocapacitor (the detailed waveform can be found in Figure S1, Supporting Information). Because of electrical source noise (here, 60 Hz) on the *I*–*V* curves (shown by the orange solid line in Figure 2b), triangular smoothing was applied to the obtained original data to reduce the noise while

© 2021 The Authors. Small Methods published by Wiley-VCH GmbH

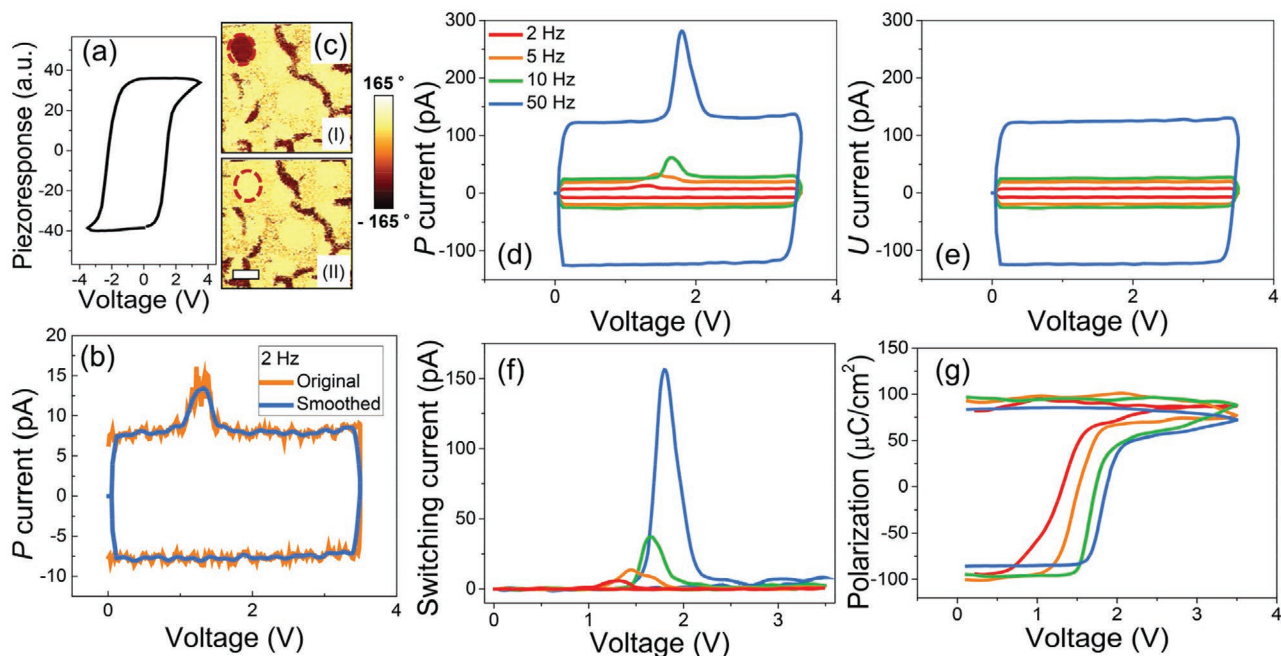

Figure 2. a) PFM hysteresis loop. b) *I–V* curves of *P* current before and after smoothing, and c) corresponding PFM images: i) before and ii) after applications of *P* and *U* waveforms, respectively. Scale bar size is 0.4 µm. Frequency-dependent *I–V* curves of d) *P* and e) *U* currents at low frequency range of 2–50 Hz, in the BFO nanocapacitors. f) Switching current and g) *P–V* hysteresis loops at low frequency range. The *I–V* curves were smoothed using the triangular smoothing method. Moreover, prior to applications of the *P* and *U* waveforms, we reset the reference state of polarization as upward direction using a reset pulse.

increasing the data visibility. Although the simplest smoothing method is rectangular smoothing, which can return the average value of the surrounding data points, triangular smoothing was used to reduce distortion of the median.[24] Five-point triangular smoothing was applied based on the following equation:

$$S_j = \frac{\left(Y_{j-2} + 2Y_{j-1} + 3Y_j + 2Y_{j+1} + Y_{j+2}\right)}{9} \tag{1}$$

where S and Y represent the smoothed and original data, respectively. Figure 2b presents a representative result of smoothing for the obtained original *P* current. The smoothing procedure was successfully performed to reduce the noise level without significantly changing the original current values (Figure 2 and Figure S1, Supporting Information). As illustrated in Figure 2d,e and Figure S2b,c (Supporting Information), the ac noises in the *P* and *U* currents were smoothed out.

Through a comparison of the *P* and *U* currents in Figure 2d,e, it is observed that the switching current peak is only visible in the *P* current. Furthermore, as the frequency increases, both the switching and non-switching currents increase as well. While the coercive voltage linearly increases with the frequency, as reported in several papers, [25,26] the polarization charge density does not show a clear dependence on the frequency (Figure 2g and Figure S1d, Supporting Information). We observed that the switched area, which was around 0.0932 μm^2 for 2 Hz, as in Figure 2c, was obtained from the PFM phase images by assuming a cylindrical shape of the switched region for converting the switching current to the polarization charge density.

To directly analyze which waveform is most advantageous for high-frequency measurements, we compared the level of non-switching current for each type of waveform. In the case of the pulse-type waveform in the previous report, [21] the non-switching current level was 0.2 nA at 2 Hz and 1.6 nA at 16 Hz under 3.6 V. The dielectric current increases proportional to rate of voltage changing (i.e., dV/dt), indicating that a non-switching current of ≈10 µA may appear at 100 kHz under the same voltage conditions, assuming that the non-switching current is entirely from the dielectric current. However, in the case of the continuous-type waveform, the non-switching current at 50 Hz was 100 pA. Specifically, the non-switching current of 200 nA will appear at 100 kHz under the same voltage conditions. This indicates that the continuous-type waveform is more suitable for high-frequency measurement because lower non-switching current is beneficial for achieving higher signal-to-noise level as discussed earlier.

Subsequently, we investigated the higher frequency range, namely 5–100 kHz, to acquire more switching current. As presented in **Figures** 3a–c, the switching and dielectric currents increase in proportion to the frequency increase. As the frequency increased, the switching current peak became broader, the level of the non-switching current became remarkably higher, and the peak voltage, which was the coercive voltage, shifted to the right side. Furthermore, the peak value of the switching current continued increasing, even at 100 kHz.

Through the switching current and the corresponding switched area (Figure S4, Supporting Information), the *P–V* hysteresis loops were acquired as presented in Figure 3d. In the *P–V* hysteresis loop, the polarization charge density was ≈75 µC cm^{-2}, which is in agreement with previous reports.[21,27,28] The value of polarization charge density in some cases may be slightly larger than the general case. This could

© 2021 The Authors. Small Methods published by Wiley-VCH GmbH

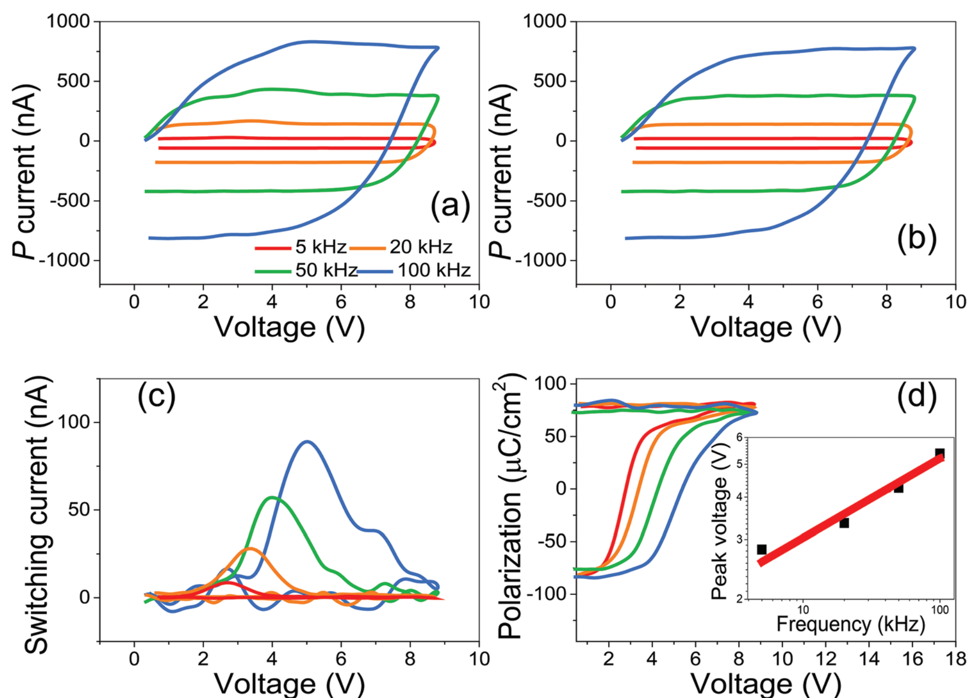

Figure 3. Frequency-dependent smoothed *I–V* curves of a) *P* and b) *U* currents. c) Switching current and corresponding d) *P–V* hysteresis loop at high frequency range (i.e., 5–100 kHz) in the BFO nanocapacitors. The inset in (d) presents coercive voltage as a function of frequency. Prior to the application of the *P* and *U* waveforms, we reset the reference state of polarization as upward direction using a reset pulse.

be because the switched area obtained from the PFM phase images may be slightly underestimated. Furthermore, the actual switched region may be larger than the cylindrical shape of the switched region. We also investigated the relationship between frequency and coercive voltage. The coercive voltage increased with increasing frequency, as presented in the inset of Figure 3d. To acquire further information, the plot of the coercive voltage versus the frequency dependence was fitted using the following equation: [26]

$$\ln(V_{cor}) = A \cdot \ln(f) + B \tag{2}$$

where V_{cor} and f represent the coercive voltage and frequency, respectively, while A and B indicate the exponent coefficient and offset, respectively. The fitting parameters, i.e., A and B, are 0.2293 and –1.043, respectively. The value of the exponential coefficient was previously reported to be around 0.05–0.23,[26,29,30] and hence is in good agreement with the obtained value in this study. Interestingly, it can be observed that the switching current gradually broadens as the frequency increases in Figure 3c. This is because, as growth of the domain wall becomes relatively slow as the frequency increases, growth of the domain wall at high frequency occurs at a relatively high voltage compared with that at low frequency. Therefore, broadening of the switching current peak occurs.[25,31]

As the present approach exhibits higher signal-to-noise ratio as well as higher measurement efficiency compared with the previously reported pulse-type low-frequency method,[21] it is possible to obtain a switching current with a relatively small area. Specifically, evaluation of ferroelectricity can be performed even on considerably smaller capacitors. Furthermore, as the high-frequency measurement can reduce leakage current, the present approach may be applicable even to relatively leaky capacitors or films.

Finally, to further evaluate the proposed method, we applied the high-frequency AFM-PUND measurements to Mo/10-nm-thick HZO film/Si nanocapacitors (further details provided in the method section). The topography image in **Figure 4**a demonstrates that the capacitor diameter is around 300–400 nm, similar to that of the BFO nanocapacitors. The PFM hysteresis loop in Figure 4b also exhibits a well-defined ferroelectric behavior, while the amplitude and phase hysteresis loops in Figure S6a,b (Supporting Information) illustrate a butterfly shape and 180 degrees of change, respectively. Furthermore, the macroscopically measured *P–V* hysteresis loop in Figure S6c (Supporting Information) demonstrates ferroelectric behavior. With this information, the AFM-PUND with 100 kHz was performed, as depicted in Figure 4c. Even with this frequency range, that is 0.01 ms, the switching current peak is clear, indicating occurrence of the switching event during application of the first waveform. However, the value of the polarization charge density given in Figure 4f is slightly smaller than that obtained macroscopically, as in Figure S6c (Supporting Information), because of the overestimated switched area based on the assumption. Notably, although the switching current is relatively small compared with that of the BFO nanocapacitor, it can be further increased by increasing the switched area.

3. Conclusion

In this work, we developed high-frequency AFM-PUND and demonstrated its application in HZO nanocapacitors at

 © 2021 The Authors. Small Methods published by Wiley-VCH GmbH

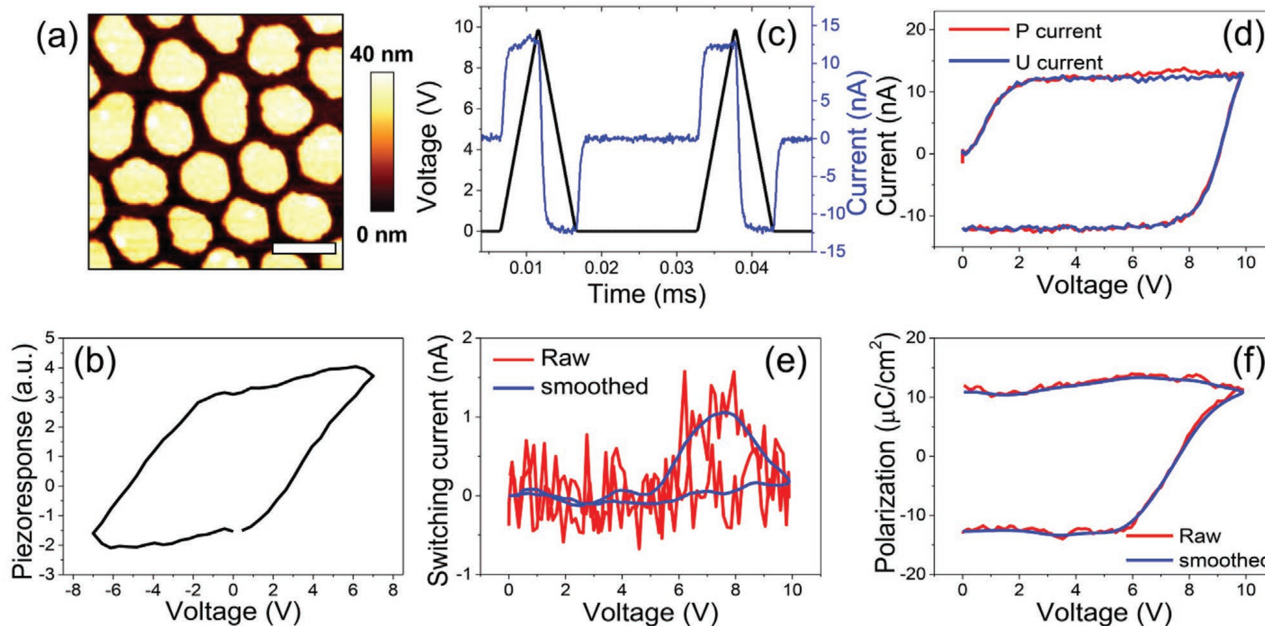

Figure 4. a) Topography image of HZO nanocapacitor. The scale bar is 0.4 µm. b) Averaged PFM hysteresis loop from 36 measurements at the same location. c) *I-t* and *V-t* curves, and corresponding d) *P* and *U* currents, e) switching current, and f) *P*–*V* hysteresis loop in the HZO nanocapacitors. The switched area was assumed using the nanocapacitor area owing to the relatively fast relaxation.

100 kHz. To increase the signal-to-noise ratio as well as the measurement efficiency, continuous waveform and simultaneous signal acquisition of the switching current were performed, while triangular smoothing was applied to the obtained *I*–*V* curves. As a result, *P*–*V* hysteresis loops were obtained in the BFO nanocapacitor at frequencies up to 100 kHz. Moreover, the method was comprehensively evaluated using emerging ferroelectric HZO nanocapacitors. High-frequency AFM-PUND can be used as a powerful and simple investigation approach for the presence of weak ferroelectricity at the nanoscale level and may potentially be operated at even higher than 100 kHz.

4. Experimental Section

BFO Nanocapacitor: An epitaxial BFO thin film with the thickness of 90 nm was grown on a $SrRuO_3$ (SRO) bottom electrode with the thickness of 75 nm. The SRO bottom electrode was deposited onto a (001)-oriented $SrTiO_3$ substrate through pulsed laser deposition. Anodic aluminum oxide shadow masks were placed on the BFO thin film. Pt top electrodes with the radius of 190 nm and thickness of 25 nm were deposited via electron-beam evaporation with the anodic aluminum oxide (AAO) template. The fabrication conditions were similar to those reported in prior studies.[32,33]

HZO Nanocapacitor: A $Hf_{0.5}Zr_{0.5}O_2$ thin film with the thickness of 10 nm was grown on a p^{++} polysilicon substrate through atomic layer deposition. Post-deposition annealing was performed via laser spike annealing at the temperature of 700 °C. To realize the HZO nanocapacitor, an AAO template with a pore size of ≈380 nm was used as a shadow mask, as reported in the previous papers. A 30-nm-thick molybdenum top electrode was deposited via e-beam evaporation through the AAO mask. A stacking configuration of Mo/HZO/Si was fabricated after mechanically removing the AAO mask. Finally, post-metallization annealing was conducted using a rapid thermal annealing process at the temperature of 350 °C for 1 min.

Measurements: A commercially available AFM (Park Systems, NX-10) was used for the entire measurement. For the PFM images in the BFO nanocapacitor, the ac voltage of 0.3 V_{peak} at 17 kHz was applied using a lock-in amplifier (Zurich Instruments, MFLI) synchronized with the AFM. *I*–*V* curves were measured using the LabVIEW program with an arbitrary waveform generator (National Instruments, PXI-5412) and a digitizer (National instruments, PXI-5122) in the capacitor (15 µF). For the measurement of AFM-PUND at low frequencies (up to 100 Hz), the inherent *I*–*V* spectroscopy mode in the AFM with a current amplifier (Femto, DLPCA-200) was used (Figures 1 and 2). At high-frequency AFM-PUND (higher than 1 kHz), the arbitrary waveform generator (Stanford Research Systems, DS345), oscilloscope mode of lock-in amplifier (Zurich instruments, MFLI), and current amplifier (Femto, DLPCA-200) were synchronized with the AFM owing to the limited frequency of the built-in *I*–*V* spectroscope in the AFM (Figures 3 and 4). In the current amplifier, transimpedance gains of 10^9 and 10^6 with the low noise mode were used for low and high-frequency measurements, respectively.[34,35] The applied voltages were 8 and 10 V of the triangular waveform, which were generated by the arbitrary waveform mode.

Supporting Information

Supporting Information is available from the Wiley Online Library or from the author.

Acknowledgements

This research was supported by the Basic Science Research Program through the National Research Foundation of Korea (NRF) funded by the Ministry of Education (No. 2019R1A6A1A03033215) and National Research Foundation of Korea (NRF) grant funded by the Korea government (MSIT) (No. 2020R1F1A1072355). This work was also supported by the Samsung Advanced Institute of Technology, SEC, in Korea. M.A. acknowledges the financial support of EPSRC (UK) through grants no. EP/T027207/1 and EP/P025803/1.

© 2021 The Authors. Small Methods published by Wiley-VCH GmbH

Conflict of Interest

The authors declare no conflict of interest.

Data Availability Statement

Research data are not shared.

Keywords

AFM-PUND, atomic force microscopy, ferroelectrics, polarization charge, positive-up-negative-down

Received: July 8, 2021
Revised: September 9, 2021
Published online:

[1] V. Garcia, M. Bibes, *Nature* **2012**, *483*, 279.
[2] H. Kohlstedt, Y. Mustafa, A. Gerber, A. Petraru, M. Fitsilis, R. Meyer, U. Böttger, R. Waser, *Microelectron. Eng.* **2005**, *80*, 296.
[3] L. Wang, W. S. Chen, J. K. Liu, J. Deng, Y. X. Liu, *Mech. Syst. Signal Process.* **2019**, *133*, 106254.
[4] J. Rodel, K. G. Webber, R. Dittmer, W. Jo, M. Kimura, D. Damjanovic, *J. Eur. Ceram. Soc.* **2015**, *35*, 1659.
[5] P. Muralt, *J. Micromech. Microeng.* **2000**, *10*, 136.
[6] N. Setter, D. Damjanovic, L. Eng, G. Fox, S. Gevorgian, S. Hong, A. Kingon, H. Kohlstedt, N. Y. Park, G. B. Stephenson, I. Stolitchnov, A. K. Taganstev, D. V. Taylor, T. Yamada, S. Streiffer, *J. Appl. Phys.* **2006**, *100*, 051606.
[7] C. Ederer, N. A. Spaldin, *Phys. Rev. Lett.* **2005**, *95*, 257601.
[8] T. Mikolajick, S. Slesazeck, M. H. Park, U. Schroeder, *MRS Bull.* **2018**, *43*, 340.
[9] S. S. Cheema, D. Kwon, N. Shanker, R. dos Reis, S. L. Hsu, J. Xiao, H. G. Zhang, R. Wagner, A. Datar, M. R. McCarter, C. R. Serrao, A. K. Yadav, G. Karbasian, C. H. Hsu, A. J. Tan, L. C. Wang, V. Thakare, X. Zhang, A. Mehta, E. Karapetrova, R. V. Chopdekar, P. Shafer, E. Arenholz, C. M. Hu, R. Proksch, R. Ramesh, J. Ciston, S. Salahuddin, *Nature* **2020**, *580*, 478.
[10] B. H. Lee, L. G. Kang, R. Nieh, W. J. Qi, J. C. Lee, *Appl. Phys. Lett.* **2000**, *76*, **1926**.
[11] H. Qiao, C. Wang, W. S. Choi, M. H. Park, Y. Kim, *Mater. Sci. Eng., R* **2021**, *145*, 100622.
[12] S. V. Kalinin, E. Karapetian, M. Kachanov, *Phys. Rev. B* **2004**, *70*, 184101.
[13] T. Tybell, C. H. Ahn, J. M. Triscone, *Appl. Phys. Lett.* **1999**, *75*, 856.
[14] A. Gruverman, M. Alexe, D. Meier, *Nat. Commun.* **2019**, *10*, 1661.
[15] O. Kwon, D. Seol, H. Qiao, Y. Kim, *Adv. Sci.* **2020**, *7*, 1901391.
[16] S. Kim, D. Seol, X. Lu, M. Alexe, Y. Kim, *Sci. Rep.* **2017**, *7*, 41657.
[17] N. Balke, S. Jesse, P. Yu, B. Carmichael, S. V. Kalinin, A. Tselev, *Nanotechnology* **2016**, *27*, 425707.
[18] Q. N. Chen, Y. Ou, F. Y. Ma, J. Y. Li, *Appl. Phys. Lett.* **2014**, *104*, 242907.
[19] N. Balke, P. Maksymovych, S. Jesse, A. Herklotz, A. Tselev, C. B. Eom, I. I. Kravchenko, P. Yu, S. V. Kalinin, *ACS Nano* **2015**, *9*, 6484.
[20] S. Martin, N. Baboux, D. Albertini, B. Gautier, *Rev. Sci. Instrum.* **2017**, *88*, 023901.
[21] O. Kwon, D. Seol, D. Lee, H. Han, I. Lindfors-Vrejoiu, W. Lee, S. Jesse, H. N. Lee, S. V. Kalinin, M. Alexe, Y. Kim, *Adv. Mater.* **2018**, *30*, 1703675.
[22] J. A. Harley, T. W. Kenny, *J. Microelectromech. Syst.* **2000**, *9*, 226.
[23] M. H. Lente, J. A. Eiras, *Ferroelectrics* **2001**, *257*, 227.
[24] W. Zucchini, Applied Smoothing Techniques. Part I: Kernel Density Estimation, http://staff.ustc.edu.cn/~zwp/teach/Math-Stat/kernel.pdf (accessed: August 2021).
[25] J. F. Scott, *Integr. Ferroelectr.* **1996**, *12*, 71.
[26] S. Hashimoto, H. Orihara, Y. Ishibashi, *J. Phys. Soc. Jpn.* **1994**, *63*, 1601.
[27] J. W. Park, S. H. Baek, P. Wu, B. Winchester, C. T. Nelson, X. Q. Pan, L. Q. Chen, T. Tybell, C. B. Eom, *Appl. Phys. Lett.* **2010**, *97*, 212904.
[28] F. Johann, A. Morelli, I. Vrejoiu, *Phys. Status Solidi B* **2012**, *249*, 2278.
[29] X. F. Chen, X. L. Dong, H. L. Zhang, F. Cao, G. S. Wang, Y. Gu, H. L. He, Y. S. Liu, *J. Am. Ceram. Soc.* **2011**, *94*, 4165.
[30] W. Li, Z. J. Chen, O. Auciello, *J. Phys. D: Appl. Phys.* **2011**, *44*, 105404.
[31] Y. Ishibashi, H. Orihara, *Integr. Ferroelectr.* **1995**, *9*, 57.
[32] Y. Kim, A. Kumar, O. Ovchinnikov, S. Jesse, H. Han, D. Pantel, I. Vrejoiu, W. Lee, D. Hesse, M. Alexe, S. V. Kalinin, *ACS Nano* **2012**, *6*, 491.
[33] Y. Kim, A. Kumar, A. Tselev, I. I. Kravchenko, H. Han, I. Vrejoiu, W. Lee, D. Hesse, M. Alexe, S. V. Kalinin, S. Jesset, *ACS Nano* **2011**, *5*, 9104.
[34] FEMTO, Datasheet of DLPCA-200, https://www.femto.de/en/products/current-amplifiers/variable-gain-up-to-500-khz-dlpca.html (accessed: August 2021).
[35] A. Gomez, Fast and direct visualization of piezo-generated charges at the nanoscale using direct piezoelectric force microscopy, https://arxiv.org/abs/1809.02339v1 (accessed: August 2021).

© 2021 The Authors. Small Methods published by Wiley-VCH GmbH